RSC Advances

RSC Publishing

PAPER

# A ZnO nanorod layer with a superior light-scattering effect for dye-sensitized solar cells

Cite this: *RSC Advances*, 2013, **3**, 18537

Rui Gao,[ab] Zhiqiang Liang,[b] Jianjun Tian,[bc] Qifeng Zhang,[b] Liduo Wang*[a] and Guozhong Cao*[bc]

Received 16th April 2013,
Accepted 29th July 2013

DOI: 10.1039/c3ra41827h

**www.rsc.org/advances**

ZnO nanorod (NR) structures have been fabricated using a precipitation method and applied as an effective scattering layer on the top of a ZnO nanoparticle (NP) electrode in a dye sensitized solar cell (DSC). This can effectively improve the light harvesting and enhance the photocurrent. Furthermore, the scattering layer decreases the charge recombination in DSCs, which is demonstrated by the results of the decreasing dark current and increasing recombination resistance. This leads to a remarkable 35% improvement in the conversion efficiency of the DSC using the ZnO nanorod scattering layer.

## 1. Introduction

Since 1991, dye-sensitized solar cells (DSCs) have been considered as an alternative to conventional solar cells due to their lower cost and easier fabrication.[1] Much attention had been focused on improving the efficiency[2–8] and stability[9–14] of DSCs. At present, the power conversion efficiencies of DSCs based on $TiO_2$ photoanodes exceed 13%.[15] The efficiency of the photoanode is a vital factor for improving the performance of DSCs, thus much study had been conducted on materials for use as photoanodes in DSCs. Mesoporous nanoparticulate semiconductor layers are well-known materials that have been applied as photoanodes in DSCs. However, the small size of the nanoparticles makes these layers transparent to visible light, and thus they only demonstrate weak light harvesting. Therefore, the effect of light scattering has been adopted as an effective means to improve the light harvesting of photoelectrodes in DSCs. This notion is based on the fact that light scattering can cause optical reflection or diffusion and, therefore, extend the travelling distance of incident light within a photoelectrode film. Light scattering in DSCs can be realized through the use of either a bilayer structure consisting of a light scattering overlayer and a nanocrystalline film, or by employing a binary combination composed of a nanocrystalline film mixed with submicron-sized particles. Various types of light scattering layer, such as photonic crystals and different large-sized metal oxide spheres, have been introduced to increase the absorption path-length of photons, create confinement properties to enhance light harvesting and decrease the probability of charge recombination.[16–18]

Besides $TiO_2$, other oxide semiconductors with wide bandgaps have also been studied, including ZnO, $SnO_2$, $Nb_2O_5$ and so on.[19–25] Among these materials, ZnO with different structures has been intensively investigated as it has an easier synthesis process and higher electron mobility compared to $TiO_2$. To date, studies concerning the enhancement of light scattering have mainly focused on $TiO_2$ photoanodes.[26–37] Methods to enhance the light scattering in photoanodes based on other materials, such as ZnO, have been ignored. In this paper, a well ordered ZnO nanorod structure with a superior light scattering effect has been developed to enhance the light capture of a photoanode based on ZnO nanoparticles, for the first time. The layer effectively enhanced the light harvesting of a ZnO film and also increased the photocurrent and conversion efficiency of DSC-based devices. This structure also allows for the suppression of the recombination of injected electrons.

## 2. Experimental

### 2.1 Fabrication of the photoanode with a light-scattering layer

ZnO nanoparticles were synthesized using a precipitation method. Firstly, 3.6 g zinc acetate dihydrate was added to distilled water (20 mL) and 1.6 g NaOH was dissolved in distilled water (500 mL) at room temperature. The solution of zinc acetate dehydrate was then poured into the NaOH solution with vigorous stirring. After 1 h, the as-obtained colloidal solution was sequentially concentrated by centrifugal separation of ZnO from the solvent and then the resulting precipitate was dispersed in distilled water (3 mL). A doctor-blade technique was used to apply the porous ZnO layer on to an FTO glass substrate and the thickness was controlled using

[a]*Key Lab of Organic Optoelectronics &Molecular Engineering of Ministry of Education, Department of Chemistry, Tsinghua University, Beijing 100084, China. E-mail: chldwang@mail.tsinghua.edu.cn*
[b]*Department of Materials Science and Engineering, University of Washington, Seattle, WA 98195, USA. E-mail: gzcao@u.washington.edu*
[c]*Beijing Institute of Nanoenergy and Nanosystems, Chinese Academy of Sciences, 100085, P.R. China. E-mail: gzcao@binn.cas.cn*

tape. After annealing at 350 °C for 30 min, the cooled nanoparticle film was transferred into a 100 mL glass bottle containing a 0.01 M $Zn(NO_3)_2$ and 0.01 M HMT aqueous solution, then heated at 80 °C for 6 h. Finally, the film was annealed at 350 °C for 30 min.

### 2.2 Assembly of the DSC devices

The cooled ZnO film was immersed in 0.3 mM N719 absolute ethanol solution for 60 min, followed by cleaning with absolute ethanol. The immersion time was optimized in an earlier work and prevents the formation of an insulating layer on the surface due to the reaction between dye molecules and ZnO.[38] The electrolyte used in this study was a liquid admixture containing 0.5 M tetrabutylammonium iodide, 0.1 M lithium iodide, 0.1 M iodine, and 0.5 M 4-*tert*-butylpyridine in acetonitrile. A chemically platinized silicon wafer was used as the counter electrode. When assembling the DSC, the electrolyte was sandwiched between the sensitized ZnO electrode and the counter electrode using two clips.

### 2.3 Characterization

The morphology of the as-synthesized ZnO nanocrystallites was characterized using scanning electron microscopy (SEM, JEOL JSM-7000) and X-ray diffraction (Philips PW1830 diffractometer), while JADE software (MDI JADE 7 materials data XRD pattern processing, identification, and quantification) was used to verify the phase and crystal structure of the ZnO films. Optical absorption (Perkin Elmer Lambda 900 UV/VIS/IR spectrometer) was used to analyze the diffuse reflectance and diffuse transmittance of the ZnO films. The photovoltaic behavior was characterized while the cell devices were irradiated using a simulated AM 1.5 sunlight with an output power of 100 mW $cm^{-2}$. An ultraviolet solar simulator (model 16S, Solar Light Co., Philadelphia, PA) with a 200 W xenon lamp power supply (Model XPS 200, Solar Light Co., Philadelphia, PA) was used as the light source, and a semiconductor parameter analyzer (4155A, Hewlett–Packard, Japan) was used to measure the current and voltage. Electrochemical impedance spectroscopy (EIS) was carried out using a Solartron 1287A coupling with a Solartron 1260 FRA/impedance analyzer to investigate the electronic and ionic processes in the DSCs.

## 3. Results and discussion

Fig. 1 (a) shows a cross sectional SEM image of a ZnO photoanode with the nanorod-based light scattering layer. As shown in the image, the whole film is 25.5 μm thick. The bilayer photoanode is composed of ZnO nanoparticles (bottom layer) and nanorods (top layer). The thicknesses of the ZnO nanoparticle and nanorod layers are about 17 and 8.5 μm, respectively. As shown in Fig. 1 (b) and (c), the ZnO nanorods are about 10 μm long and 1 μm wide, coating the nanoparticles in different directions, which effectively enhances the light reflectance of the photoanode film. As shown in Fig. 1 (d), the ZnO nanoparticles synthesized using the precipitation method are about 30–40 nm, so they should absorb dye effectively. Moreover, the nanoparticles are relatively larger than those commonly used (10–20 nm) and enable better dye permeation from the top of film to the bottom.[39,40]

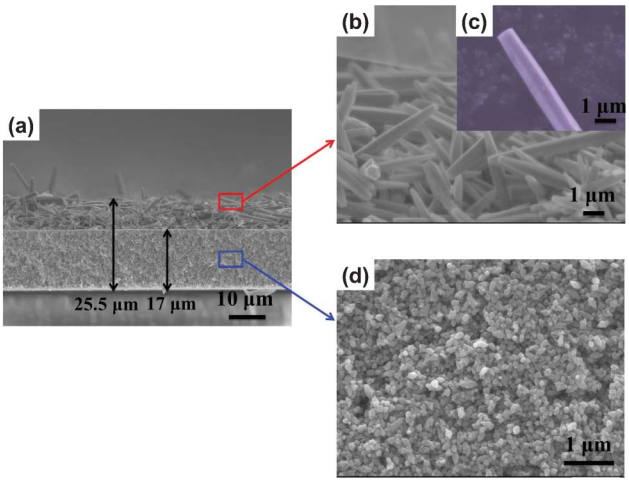


**Fig. 1** SEM images of: (a) the bilayer structure composed of a ZnO nanoparticle under-layer and a top-layer of nanorods; (b) and (c) cross sections of the nanorods; and (d) a cross section of the nanoparticles.

Fig. 2 shows the XRD spectra of the ZnO nanoparticles and nanorods. The XRD peaks can be indexed to those of standard ZnO nanoparticles and nanorods very well (Joint Committee on Powder Diffraction Standards (JCPDS) card number: 36-1451). As shown in Fig. 2, for the nanoparticles the peak intensity follows the order (101) > (100) > (002). This is due to the surface energies ($E$) of the facets in the ZnO crystals, which follow the sequence $E(101) > E(100) > E(002)$; the same order as the crystal growth rates at low temperature.[41–43] After the nanorod light scattering layer was applied, the relative intensity of the (002) peak notably increased. This is due to

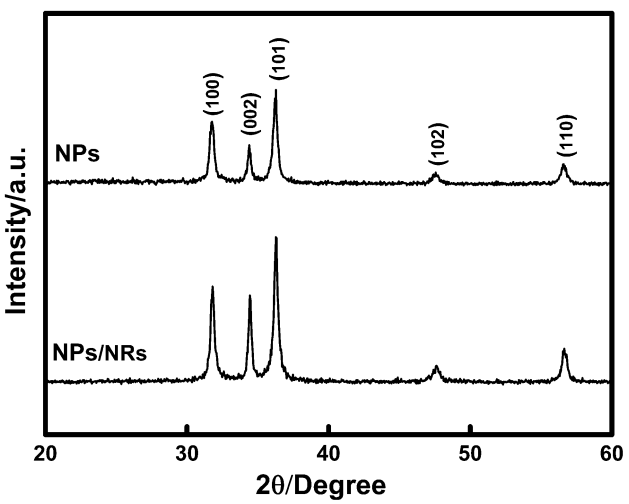


**Fig. 2** XRD patterns of the electrodes based on ZnO nanoparticles and nanoparticles coated with light-scattering nanorods.

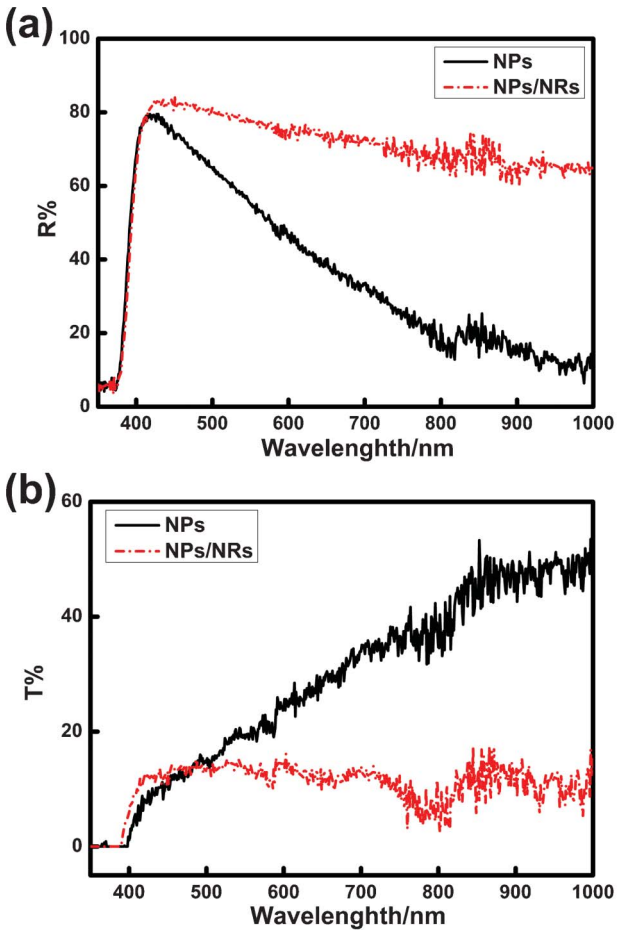


**Fig. 3** (a) UV-vis diffuse reflectance and (b) diffuse transmittance spectra of the ZnO nanoparticle and nanoparticle/nanorod electrodes.

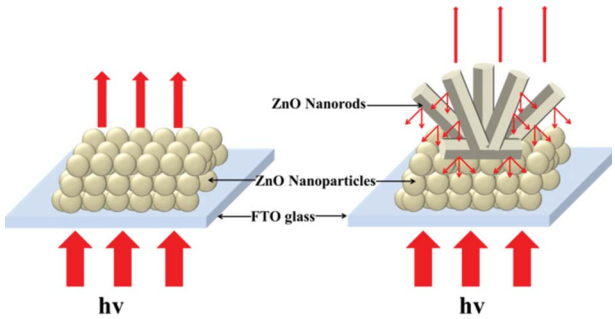


**Scheme 1** Schematic diagram of the light scattering effects in the ZnO nanoparticle and nanoparticle/nanorod electrodes.

$E$(002) being increased because the nanorods were obtained at 80 °C, a much higher temperature than that used to obtain the nanoparticles. Furthermore, the crystal size of the ZnO nanoparticles and nanorods can be estimated using the Scherrer equation. The crystal size calculated from the two different spectra are 30 nm and 27 nm, respectively. This result indicates that the crystal size of the nanorods is smaller than that of nanoparticles, which is due to the faster growth rate at higher temperature.

For high performance photoanodes of DSCs, efficient light scattering is needed to increase the probability of incident photons being absorbed. Therefore, light-scattering is an important property of photoanodes that can influence the performance of DSCs. Diffuse reflectance and transmittance data can reveal the extent to which incident light is scattered by particles in the photoanode and how much incident light passes through the photoanode without being scattered. The ideal light scattering properties of a photoanode should be a high diffuse reflectance and low diffuse transmission. As shown in Fig. 3 (a), compared to the control ZnO nanoparticle film, the diffuse reflectance of the film coated with a ZnO nanorod-based scattering layer is much stronger in the 400–800 nm range, which is the main wavelength range that dyes used in DSCs can effectively capture photons. Within this wavelength range, a light diffuse reflectance of 70–80% was achieved for the film coated with nanorods, which was remarkably better than that of the ZnO nanoparticles. As proposed in Scheme 1, this remarkable reflectance can obviously be attributed to the strong scattering of the nanorods, which make the incident light directly reflect back towards the nanoparticles when illumination is applied. Fig. 3 (b) shows that the diffuse transmittance of the ZnO film coated with nanorods is much weaker than that of the nanoparticle film, possessing a stronger ability to trap photons in the photoanode film. As a result, incident light could be scattered more efficiently by the ZnO film coated with the nanorod scattering layer. Furthermore, the photocurrent and conversion efficiency of the device based on the ZnO film coated with nanorods are expected to be increased by the enhanced light scattering.

The photoanodes with and without the ZnO nanorod scattering layer were subsequently assembled into DSC devices, in order to investigate the effect of the light scattering on the photovoltaic performance. As shown in Fig. 4, the incident photon-to-current efficiency (IPCE) spectra of the ZnO nanoparticle and nanoparticle/nanorod electrodes were obtained. It should be noted that the IPCE of the device based on the ZnO film coated with the nanorod light scattering layer is higher than that based on the ZnO film without the scattering layer in the 500–700 nm range, which is the main absorption range of the N719 dye. In particular, there is an obvious enhancement of IPCE in the wavelength range between 600–700 nm when the nanorods layer is coated onto the ZnO particles film, which could be due to the superior light scattering effect of such a nanorods layer. The enhanced IPCE should cause an increase in the devices' photocurrent.

As shown in Fig. 5 (a) and Table 1, compared to the control sample of ZnO nanoparticles, the short-circuit current density ($J_{sc}$) of the device based on the film coated with nanorods increased from 7.92 mA $cm^{-2}$ to 9.31 mA $cm^{-2}$, which is a relative enhancement of 19%. As discussed above, the increased photocurrent density is due to the much stronger light scattering of the ZnO nanorod coating. These results also agree with the results of the IPCE enhancement shown in

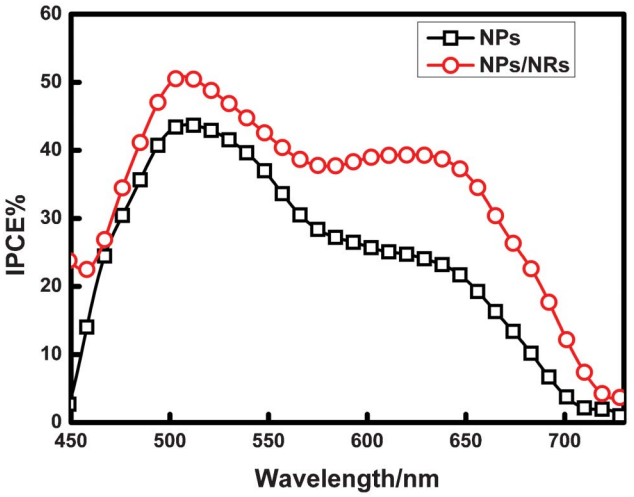


**Fig. 4** IPCE spectra of DSC devices based on ZnO nanoparticle and nanoparticle/nanorod electrodes.

Fig. 4. The amount of dye-loading in the ZnO films with and without the scattering layer was tested by desorbing the dye from the ZnO film using NaOH solution. As shown in Table 1,

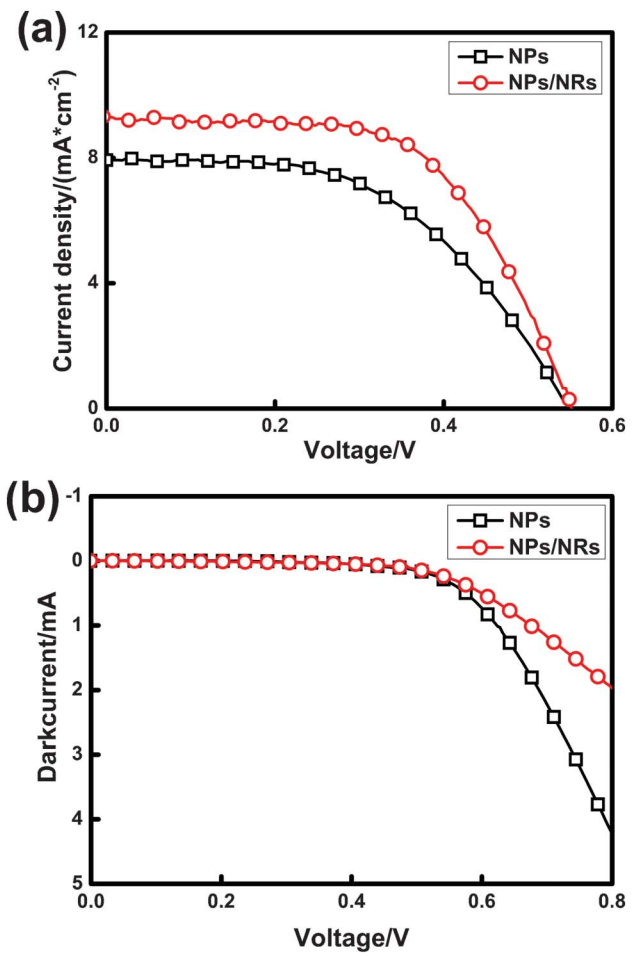


**Fig. 5** (a) *I–V* curve and (b) dark current curve of the DSC devices based on ZnO nanoparticle and nanoparticle/nanorod electrodes.

**Table 1** Photo-voltaic parameters of the devices based on different types of ZnO photoanode

| Samples | $V_{oc}$ (V) | $J_{sc}$ (mA cm$^{-2}$) | FF | $\eta$ (%) | Dye-loading (nmol cm$^{-2}$) |
|---|---|---|---|---|---|
| NPs | 0.55 | 7.92 | 0.52 | 2.25 | 108 |
| NPs/NRs | 0.55 | 9.31 | 0.59 | 3.03 | 115 |

the dye-loading increased slightly from 108 to 115 nmol cm$^{-2}$ after the light scattering layer was coated on to the film. This slight increase in the dye-loading is much smaller than the enhancement of $J_{sc}$, indicating that the increase in the photocurrent is largely not due to enhanced dye-loading, but rather the stronger light scattering effect of the layer of nanorods coated on to the ZnO nanoparticle film. Besides $J_{sc}$, the fill factor (FF) of the DSC device with the nanorod scattering layer is also higher compared with the device based on the nanoparticles. As shown in Table 1, the FF increased from 0.52 to 0.59. As a result, the conversion efficiency of the device based on the film coated with the nanorod scattering layer exhibited a remarkable 35% enhancement, increasing from 2.25% to 3.03% under AM 1.5, 100 mW cm$^{-2}$ illumination and showing a much better performance than the device based on ZnO nanoparticles. As shown in Fig. 5 (b), the dark current of the device based on the film coated with a nanorod scattering layer obviously decreased compared to that based on ZnO nanoparticles, indicating a lower charge recombination from the conduction band of ZnO to the redox couple in the electrolyte. The decreased charge recombination could be explained by two reasons: Firstly, the layer of ZnO nanorods decreased the surface area of the nanoparticles in contact with the electrolyte, thus decreasing charge recombination. Secondly, the ZnO light scattering layer is obtained using an *in situ* method, therefore the surface state could be suppressed in such a process.

To further investigate the effects of charge transport and recombination in the two different photoanodes, electrochemical impedance spectroscopy (EIS) was conducted on the devices based on the differently structured ZnO materials. EIS is a well-established technique for characterizing DSCs, which demonstrates all of the kinetic processes of DSCs such as electron transport in the photoanode, recombination at the oxide/electrolyte interface, charge transfer at the counter electrode/electrolyte interface, and electron diffusion in the electrolyte.[44–47] We have mainly focused on charge recombination, which occurs around $10^1$ Hz.

Fig. 6 (a) shows Nyquist plots of the DSC devices based on the ZnO nanoparticle and nanoparticle/nanorod electrodes under dark conditions. It can be seen in Fig. 6 (a) that the value of $R_{ct}$, represented by the radius of the middle semicircle, obviously increased after coating with the nanorod scattering layer. In the dark, this represents the resistance of charge recombination at the ZnO/dye/electrolyte interface. Therefore, back reaction decreased. This result is also in accordance with the results of the decreasing dark current measurements, shown in Fig. 5 (b).

 

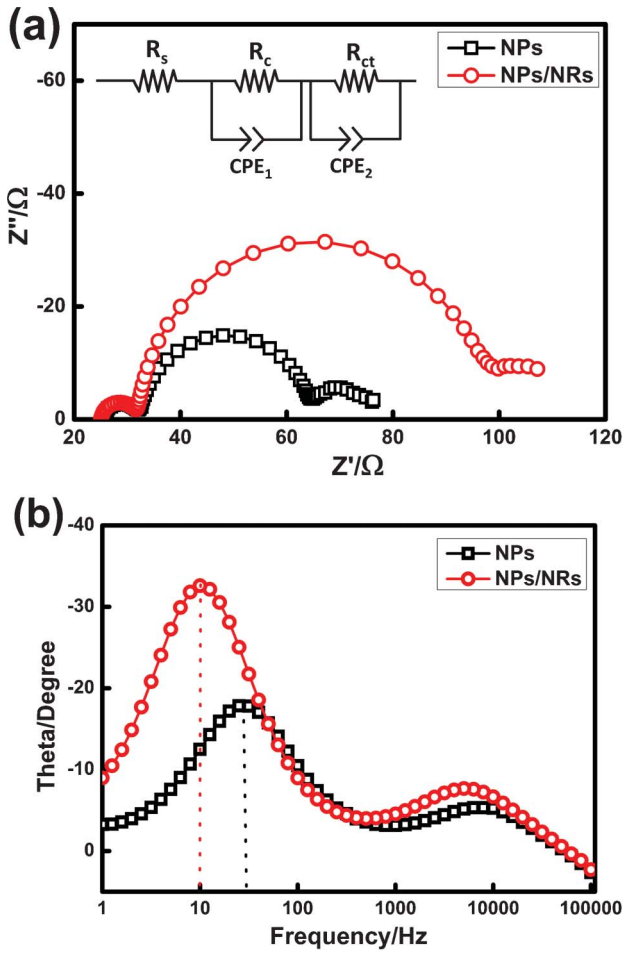


**Fig. 6** (a) Nyquist and (b) Bode plots of the DSC devices based on ZnO nanoparticle and nanoparticle/nanorod electrodes under dark conditions.

The series resistance ($R_s$) is well-known as a key factor that affects the FF. $R_s$ is mainly composed of the resistance of the conductive glass, the resistance of the electron transport within ZnO and the bulk resistance of the electrolyte. The following five equations reveal the relationship between FF and $R_s$.[45] In eqn (1), $R_{ch}$ represents the characteristic resistance of the solar cell. In eqn (2), $R_s$ and $r_s$ represent the series resistance and the normalized series resistance, respectively. In eqn (3), $v_{oc}$ is defined using the normalized $V_{oc}$, where $k$ is the Boltzmann constant and $T$ is the temperature in Kelvin.[48] In eqn (4), $FF_0$ denotes the idealized fill factor, which could be considered to be the same for the devices with the two different photoanodes, because $V_{oc}$ does not change significantly.

$$R_{ch} \approx \frac{V_{oc}}{J_{sc}} \quad (1)$$

$$r_s = \frac{R_s}{R_{ch}} \quad (2)$$

$$v_{oc} = \frac{q}{nkT} \times V_{oc} \quad (3)$$

$$FF_0 = \frac{v_{oc} - \ln(v_{oc} + 0.72)}{v_{oc} + 1} \quad (4)$$

$$FF = FF_0 \times (1 - r_s) \quad (5)$$

The values of $R_s$ can be calculated using the fit obtained from Z-view software, and are about 32 and 23 Ω for the nanoparticle and nanoparticle/nanorod photoanodes, respectively. The values of $R_{ch}$ can be calculated from the results shown in Table 1, which are 139 and 118 Ω for nanoparticle and nanoparticle/nanorod photoanodes, respectively. Next, the values of $r_s$ for the nanoparticle and nanoparticle/nanorod photoanodes could be obtained based on the above results, which are 0.23 and 0.19, respectively. From eqn (5), due to the fact that $FF_0$ can be considered to be the same for the devices based on nanoparticles and nanoparticle/nanorod photoanodes, FF is increased when the nanorod scattering layer is applied. Bode plots of the devices based on the nanoparticle and nanoparticle/nanorod photoanodes are shown in Fig. 6 (b). There are three peaks in the phase of the spectrum associated with the three transient processes in the DSCs. The middle-frequency peak (in the 10–100 Hz range) was derived from the lifetime of the electrons in the ZnO, as shown in the following equation[46]:

$$\tau = \frac{1}{2\pi f_{peak}} \quad (6)$$

As shown in Fig. 6 (b), the frequency of the minimum phase angle peak of the device based on the film with the ZnO nanorod scattering layer shifts to a lower value (10 Hz) compared to that based on the ZnO nanoparticles (28 Hz). As a result, from eqn (6), the lifetime of the electrons in the conduction band was enhanced by using the ZnO nanorod scattering layer. This result means that it is more difficult for the electrons in the conductive band of ZnO to recombine with the redox couple in the electrolyte. This is also in accordance with the results of the decreasing dark current shown in Fig. 5 (b).

The diffusion resistance ($R_d$), which represents the effective charge transport occurring by diffusion along the ZnO network, could not be distinguished from $R_c$ and $R_{ct}$ under these conditions because $R_d$ overlaps with $R_c$ and $R_{ct}$ at the position where the transition from $R_c$ to $R_{ct}$ occurs. However, with a decrease in the bias voltage of the open circuit conditions, a diffusion resistance similar to that observed for Warburg-like diffusion starts to appear along with an increase in $R_{ct}$.[44] Separating $R_d$ from $R_{ct}$ is useful for investigating the charge transport properties of the ZnO photoanodes. The electron diffusion coefficient ($D_n$) can be calculated from the following equation using the values of $R_d$ and the chemical capacitance ($C_\mu$)[47]:

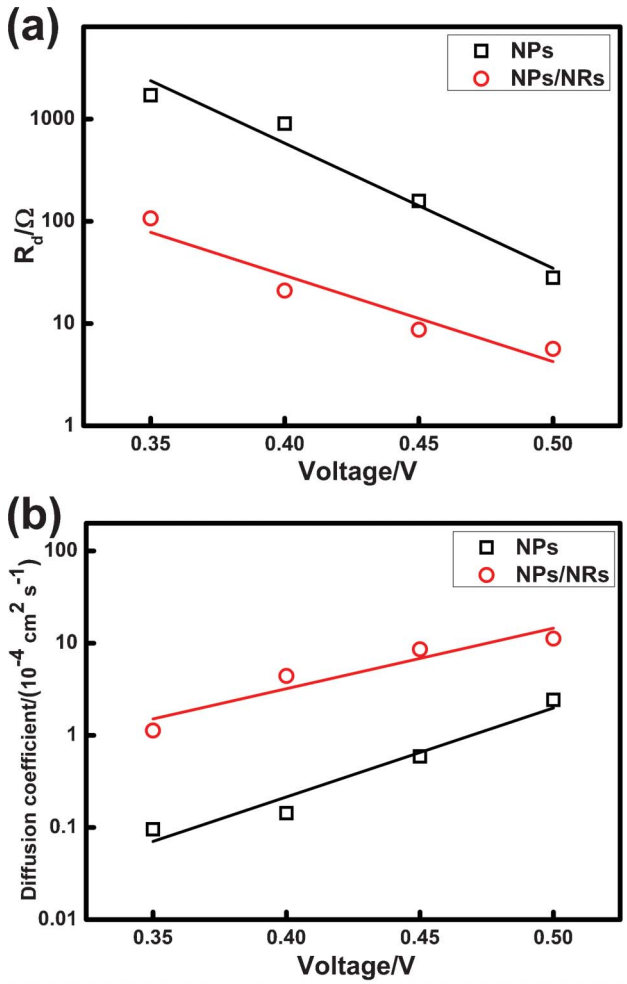


**Fig. 7** (a) The diffusion resistance and (b) electron diffusion coefficient of the DSC devices based on ZnO nanoparticle and nanoparticle/nanorod electrodes at a low bias voltage and under dark conditions.

$$D_n = \frac{L^2}{R_d \times C_\mu} \quad (7)$$

where $L$ is the film thickness, $R_d$ is the diffusion resistance and $C_\mu$ is the chemical capacitance, which could be obtained using Z-View software.

As shown in Fig. 7(a), $R_d$ notably decreased when the ZnO NR scattering layer was applied. This result means that the scattering layer decreases the diffusion resistance, resulting in faster electron diffusion. As shown in Fig. 7(b), $D_n$ notably increased as the ZnO NR scattering layer was applied, demonstrating faster electron diffusion in the bilayer photoanode composed of ZnO NPs and NRs.

## 4. Conclusions

In summary, micrometer sized ZnO nanorods have been developed as a light scattering layer in ZnO based DSCs, for the first time. The advantages of using such a scattering layer can be summarized as follows: (i) improved light scattering, which has been confirmed by the enhanced diffuse reflection. The efficient light scattering layer can also localize the incident light within the electrode and enhance the photocurrent. (ii) Decreased charge recombination and improved electron diffusion in DSCs, which could be observed from the results of the increased recombination resistance and electron diffusion coefficient. This leads to a remarkable improvement in the conversion efficiency of the DSC using a ZnO nanorod scattering layer.

## Acknowledgements

This work has been supported in part by the US Department of Energy, Office of Basic Energy Sciences, Division of Materials and Engineering under Award No. DE-FG02-07ER46467 (Q. F. Z.) for the microstructure characterization and for some of the power conversion efficiency measurements, National Science Foundation (DMR-1035196), the National Natural Science Foundation of China under Grant No. 51273104 and the National Key Basic Research and Development Program of China under Grant No. 2009CB930602. R. Gao would also like to thank the China Scholarship Council (CSC) for providing a scholarship for the PhD study at the University of Washington.

## Notes and references

1 B. Oregan and M. Grätzel, *Nature*, 1991, **353**, 737.
2 D. Kuang, C. Klein, S. Ito, J.-E. Moser, R. Humphry-Baker, S. M. Zakeeruddin and M. Graetzel, *Adv. Funct. Mater.*, 2007, **17**, 154.
3 R. Gao, G. D. Niu, L.-D. Wang, B.-B. Ma and Y. Qiu, *Acta Phys.-Chim. Sin.*, 2013, **29**, 73.
4 R. Gao, L. Wang, B. Ma, C. Zhan and Y. Qiu, *Langmuir*, 2010, **26**, 2460.
5 R. Gao, B.-B. Ma, L.-D. Wang, Y.-T. Shi, H.-P. Dong and Y. Qiu, *Acta Phys.-Chim. Sin.*, 2011, **27**, 413.
6 R. Gao, L. Wang, Y. Geng, B. Ma, Y. Zhu, H. Dong and Y. Qiu, *Phys. Chem. Chem. Phys.*, 2011, **13**, 10635.
7 R. Gao, L. Wang, Y. Geng, B. Ma, Y. Zhu, H. Dong and Y. Qiu, *J. Phys. Chem. C*, 2011, **115**, 17986.
8 R. Gao, Z. Liang, J. Tian, Q. Zhang, L. Wang and G. Cao, *Nano Energy*, 2013, **2**, 40.
9 Q. B. Meng, K. Takahashi, X. T. Zhang, I. Sutanto, T. N. Rao, O. Sato, A. Fujishima, H. Watanabe, T. Nakamori and M. Uragami, *Langmuir*, 2003, **19**, 3572.
10 E. Figgemeier and A. Hagfeldt, *Int. J. Photoenergy*, 2004, **6**, 127.
11 P. M. Sommeling, M. Spath, H. J. P. Smit, N. J. Bakker and J. M. Kroon, *J. Photochem. Photobiol., A*, 2004, **164**, 137.
12 S. Nakade, T. Kanzaki, S. Kambe, Y. J. Wada and S. Yanagida, *Langmuir*, 2005, **21**, 11414.
13 M. Gratzel, *C. R. Chim.*, 2006, **9**, 578.
14 A. R. S. Priya, A. Subramania, Y.-S. Jung and K.-J. Kim, *Langmuir*, 2008, **24**, 9816.
15 A. Yella, H. W. Lee, H. N. Tsao, C. Y. Yi and A. K. Chandiran, *Science*, 2011, **334**, 1203.

 

16 H.-J. Koo, Y. J. Kim, Y. H. Lee, W. I. Lee, K. Kim and N.-G. Park, *Adv. Mater.*, 2008, **20**, 195.
17 J. Qian, P. Liu, Y. Xiao, Y. Jiang, Y. Cao, X. Ai and H. Yang, *Adv. Mater.*, 2009, **21**, 3663.
18 Z. Tian, H. Tian, X. Wang, S. Yuan, J. Zhang, X. Zhang, T. Yu and Z. Zou, *Appl. Phys. Lett.*, 2009, **94**, 031905.
19 R. Gao, J. Tian, Z. Liang, Q. Zhang, L. Wang and G. Cao, *Nanoscale*, 2013, **5**, 1894.
20 G. Redmond, D. Fitzmaurice and M. Graetzel, *Chem. Mater.*, 1994, **6**, 686.
21 H. Rensmo, K. Keis, H. Lindstrom, S. Sodergren, A. Solbrand, A. Hagfeldt, S. E. Lindquist, L. N. Wang and M. Muhammed, *J. Phys. Chem. B*, 1997, **101**, 2598.
22 K. Sayama, H. Sugihara and H. Arakawa, *Chem. Mater.*, 1998, **10**, 3825.
23 K. Keis, E. Magnusson, H. Lindstrom, S. E. Lindquist and A. Hagfeldt, *Sol. Energy Mater. Sol. Cells*, 2002, **73**, 51.
24 T. Stergiopoulos, I. M. Arabatzis, H. Cachet and P. Falaras, *J. Photochem. Photobiol., A*, 2003, **155**, 163.
25 N. G. Park, M. G. Kang, K. S. Ryu, K. M. Kim and S. H. Chang, *J. Photochem. Photobiol., A*, 2004, **161**, 105.
26 G. Zhu, L. Pan, J. Yang, X. Liu, H. Sun and Z. Sun, *J. Mater. Chem.*, 2012, **22**, 24326.
27 H. Yu, Y. Bai, X. Zong, F. Tang, G. Q. Lu and L. Wang, *Chem. Commun.*, 2012, **48**, 7386.
28 T. T. Trang Pham, T. Bessho, N. Mathews, S. M. Zakeeruddin, Y. M. Lam, S. Mhaisalkar and M. Grätzel, *J. Mater. Chem.*, 2012, **22**, 16201.
29 W. Peng and L. Han, *J. Mater. Chem.*, 2012, **22**, 20773.
30 H. Pang, H. Yang, C. X. Guo, J. Lu and C. M. Li, *Chem. Commun.*, 2012, **48**, 8832.
31 W. Kwon, Y.-J. Chang, Y.-C. Park, H. M. Jang and S.-W. Rhee, *J. Mater. Chem.*, 2012, **22**, 6027.
32 K. S. Kim, H. Song, S. H. Nam, S. M. Kim, H. Jeong, W. B. Kim and G. Y. Jung, *Adv. Mater.*, 2012, **24**, 792.
33 H. Kim do, H. J. Koo, J. S. Jur, M. Woodroof, B. Kalanyan, K. Lee, C. K. Devine and G. N. Parsons, *Nanoscale*, 2012, **4**, 4731.
34 Q. Zhang, C. S. Dandeneau, K. Park, D. Liu, X. Zhou, Y.-H. Jeong and G. Cao, *J. Nanophotonics*, 2010, **4**, 041540.
35 L. Song, H. Bin Yang, X. Wang, S. Y. Khoo, C. C. Wong, X.-W. Liu and C. M. Li, *ACS Appl. Mater. Interfaces*, 2012, **4**, 3712.
36 S. Dadgostar, F. Tajabadi and N. Taghavinia, *ACS Appl. Mater. Interfaces*, 2012, **4**, 2964.
37 Z.-H. Liu, X.-J. Su, G.-L. Hou, S. Bi, Z. Xiao and H.-P. Jia, *J. Power Sources*, 2012, **218**, 280.
38 T. P. Chou, Q. Zhang and G. Cao, *J. Phys. Chem. C*, 2007, **111**, 18804.
39 Y. Shi, C. Zhan, L. Wang, B. Ma, R. Gao, Y. Zhu and Y. Qiu, *Adv. Funct. Mater.*, 2010, **20**, 437.
40 Y. Shi, C. Zhu, L. Wang, W. Li, C. Cheng, K. M. Ho, K. K. Fung and N. Wang, *J. Mater. Chem.*, 2012, **22**, 13097.
41 L. Xu, Y.-L. Hu, C. Pelligra, C.-H. Chen, L. Jin, H. Huang, S. Sithambaram, M. Aindow, R. Joesten and S. L. Suib, *Chem. Mater.*, 2009, **21**, 2875.
42 K. X. Yao and H. C. Zeng, *J. Phys. Chem. B*, 2006, **110**, 14736.
43 X. Jiang, C. L. Jia and B. Szyszka, *Appl. Phys. Lett.*, 2002, **80**, 3090.
44 Q. Wang, S. Ito, M. Graetzel, F. Fabregat-Santiago, I. Mora-Sero, J. Bisquert, T. Bessho and H. Imai, *J. Phys. Chem. B*, 2006, **110**, 25210.
45 T. Hoshikawa, R. Kikuchi and K. Eguchi, *J. Electrochem. Soc*, 2006, **588**, 59.
46 Q. Wang, J. Moser and M. Gratzel, *J. Phys. Chem. B*, 2005, **109**, 14945.
47 J. Bisquert, *J. Phys. Chem. B*, 2002, **106**, 325.
48 D. Qin, Y. Zhang, S. Huang, Y. Luo, D. Li and Q. Meng, *Electrochim. Acta*, 2011, **56**, 8680.